Chemistry and kinetics of the interaction of hydrogen atoms with (100) InP surfaces: An *in situ* real-time ellipsometric study

G. Bruno, P. Capezzuto, and M. Losurdo
Centro di Studio per la Chimica dei Plasmi–CNR, Dipartimento di Chimica-Università di Bari-via Orabona, 4-70126 Bari, Italy
(Received 7 February 1996; revised manuscript received 27 June 1996)

The interaction of InP surfaces with H atoms is investigated in the afterglow region of H_2 radio-frequency (rf) plasmas by *in situ* real-time spectroscopic ellipsometry (SE). The effect of the InP surface temperature and the hydrogen plasma exposure time on the native-oxide reduction and phosphorus-depletion processes is studied. The morphology and composition of the InP surface resulting from these two competing processes is well characterized by spectroscopic ellipsometry. Typically complete removal of oxygen is obtained at 230 °C after 7 minutes of plasma exposure without damage due to phosphorus depletion. The applicability of real-time ellipsometry to determine precisely the optimum cleaning end point is well demonstrated. The chemistry and kinetics of both oxygen removal and phosphorus depletion are described and the corresponding pseudoactivation energies are derived. [S0163-1829(96)08947-3]

I. INTRODUCTION

Presently, there is a great interest in developing new techniques for the native-oxide removal and the cleaning processes of III-V semiconductor surfaces. This research is driven by both the limitations of conventional wet-etching procedures[1] and the desire to develop dry methods compatible with a vacuum environment during device manufacturing.

In situ hydrogen plasma cleaning seems to be attractive, since atomic hydrogen generated by a plasma can efficiently reduce carbon contaminations and native oxides,[2] giving good-quality III-V surfaces for epitaxial growth. Moreover, the hydrogen plasma treatment offers the advantage of a simultaneous passivation of III-V surface,[3,4] i.e., blocking the electrical activity of dangling bonds, impurities, and nonradiative electron traps, yielding an increase of the photoluminescence (PL) efficiency.[5,6]

However, dealing particularly with the InP material, it is well documented that H atoms can induce decomposition of InP substrate,[7] depending on H-atom dose,[8–10] plasma exposure time,[11–13] and surface temperature.[14]

This difficulty in getting good InP surfaces can be due to the fact that the interaction of hydrogen atoms with the InP surface may either lead to oxygen removal for the reduction of native oxide

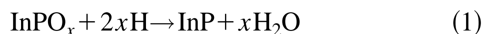

$$InPO_x + 2xH \rightarrow InP + xH_2O \quad (1)$$

or to phosphorus depletion via the production of PH_3,

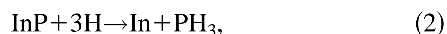

$$InP + 3H \rightarrow In + PH_3, \quad (2)$$

which causes formation of metallic indium.

In addition, H atoms act on the material by passivating various kinds of defects (d) through the very fast process

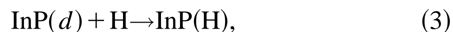

$$InP(d) + H \rightarrow InP(H), \quad (3)$$

which imparts a reduced surface and bulk density of states and, hence, improved optoelectronic properties.

The experimental conditions separating the two reaction types, i.e., the ''reaction boundary'' between O removal and P depletion, have not yet been defined. Thus, *in situ* diagnostics and real-time control of the oxide-reduction process and of the effects induced by H atoms on the InP morphology are needed. Unfortunately, many of the usual surface techniques (RHEED, RBS, SEM, TEM, XPS, etc.) are destructive or are not ambient gas compatible or are both and, hence, cannot operate during processing. On the contrary, ''new'' optical diagnostics such as spectroscopic ellipsometry (SE), attenuated total reflection Fourier transform infrared spectroscopy[15] (ATRFTIR) and photoluminescence (PL)[15–17] are nondestructive and noninvasive techniques which offer great promise for the *in situ* real-time monitoring of a wide variety of processes such as growth, oxidation, surface cleaning, etching, and also for the simultaneous optical, microstructural, and compositional characterization of the processed material with a monolayer sensitivity. However, a PL detection system cannot operate at sample temperatures higher than room temperature. This obstacle can be overcome by using *in situ* real-time spectroscopic ellipsometry which can operate at sample temperatures much higher than room temperature. Therefore, the description of the temperature effect on the surface chemistry during the hydrogen plasma cleaning of InP surface is the main objective of the present study. Spectroscopic ellipsometry and single-wavelength ellipsometry (SWE) are widely utilized for the *in situ* real-time layer-by-layer characterization of the growth and processing of multilayers structures using (MBE), (MOCVD) and plasma-assisted systems.[18–20] As an example, *in situ* SE has allowed, on one hand, the study of the kinetics of the O-removal in the system Si/SiO_2 (Refs. 21 and 22) and of the InP surface oxidation[23,24] and, on the other hand, the evaluation of the quality of the resulting surface.

In this paper, we report on the use of spectroscopic phase-modulated ellipsometry to investigate *in situ* the interaction of atomic hydrogen, present in the remote zone of H_2 radio-frequency (rf) plasmas, with (100) InP surfaces covered by native oxide. The influence of surface temperature and of H-atom exposure time on the kinetics of both the oxide re-

 © 1996 The American Physical Society

moval and phosphorus depletion and also on the InP surface morphology are investigated and discussed. The efficiency of rf hydrogen remote plasmas as an *in situ* cleaning technique in producing high-quality reproducible and clean InP surfaces for epitaxial growth is demonstrated. Moreover, an optimum surface temperature range is found where P depletion can be minimized and high cleanliness without surface damage can be achieved. The end-point detection of the cleaning process is well shown by *in situ* real-time ellipsometry.

II. EXPERIMENT

A. Architecture of the remote plasma reactor. InP treatment experiments

The cleaning experiments were performed in a homemade remote-plasma MOCVD (RP-MOCVD) apparatus specifically designed for the MOCVD epigrowth of III-V materials and previously described in detail in Ref. 25. Basically, it consists of a quartz plasma tube, where the plasma was ignited between two semicircular external electrodes, and a stainless steel MOCVD reactor, where the InP sample was positioned on a molybdenum susceptor, 10 cm away from the plasma tube end in order to minimize radiative damage by ion bombardment. A load lock chamber was used to introduce samples in the MOCVD reactor to avoid exposure to air contamination. All the apparatus was evacuated by turbomolecular pumps to a base vacuum of 10^{-8} torr.

The hydrogen plasma was operated at 13.56 MHz with the input rf power of 60 W, the H_2 gas flow rate of 800 sccm, and the pressure of 1 torr.

Under the above plasma conditions, the H-atom density in the afterglow region was estimated to be $[H]=10^{15}$ cm^{-3} at the substrate position, corresponding to a H-atom flux of 4×10^{20} atoms/cm^2 sec impinging on the (100) SI (Fe-doped) InP surface.[26] The hydrogen exposure time varied from 1 min to 5 h.

The effect of surface temperature on the oxygen-removal and phosphorus-depletion processes was investigated by varying the substrate temperature from 25 to 350 °C, while for the thermal annealing experiments the temperature increased to 640 °C. The substrate was radiatively heated and its temperature was measured with a K thermocouple fixed to the sample holder and checked by an optical pyrometer.

To compare the efficiency of the present dry-cleaning procedure with the more common wet-etching methods, some InP substrates were at first washed with isopropanol and rinsed in DI water and afterwards etched in a H_2SO_4:H_2O_2:H_2O (8:1:1) solution for 2 min at room temperature.

B. *In situ* ellipsometry: Measurements and data analysis

In situ spectroscopic ellipsometry in the near-ultraviolet (UV)-visible range (1.5–5.5 eV) is a powerful technique to study surface modifications because of its high sensitivity to surface morphology and to layer thickness and composition through the spectral dependence of the dielectric response.

The phase-modulated spectroscopic ellipsometer (UVISEL by ISA-Jobin Yvon)[27–29] is assembled on the MOCVD chamber through conflat strain-free quartz windows flanges. The alignment of the SE optical components and the electronic calibration have been performed according to the procedure described in detail in Ref. 28. The accuracy of the present alignment and calibration and of SE measurements has been tested by recording SE spectra of Si/SiO_2 standard sample, and can also be deduced by the comparison of the c-InP database (provided by Aspnes) with our best InP spectrum (see Fig. 2).

Briefly, spectroscopic ellipsometry measures the energy dependence of the ratio, ρ, between the complex reflectance coefficients of the two components of the polarized light, r_p and r_s, respectively, parallel and perpendicular to the plane of incidence:

$$\rho=\frac{r_p}{r_s}=\tan\Psi e^{i\Delta}, \tag{4}$$

where Ψ is the amplitude ratio ($\tan\Psi=|r_p|/|r_s|$), and Δ is the phase difference ($\Delta=\delta_p-\delta_s$) between the p and s components. The pseudodielectric function, $\langle\epsilon\rangle$, can be derived from the ρ parameter through the equation

$$\langle\epsilon\rangle=\langle\epsilon_1\rangle+i\langle\epsilon_2\rangle=\epsilon_0\sin^2\phi_0\left[1+\tan^2\phi_0\frac{(1-\rho)^2}{(1+\rho)^2}\right], \tag{5}$$

where ϵ_0 is the ambient dielectric function and ϕ_0 is the light incidence angle (71.8° in our experiments). The analysis of the SE spectra is based on the Bruggemann effective medium approximation (BEMA),[30] which allows the description of the dielectric function, ϵ, of a composite material through the dielectric function, ϵ_i, and volume fraction, f_i, of its ith components, by the formula

$$\sum_i f_i\frac{\epsilon_i-\epsilon}{\epsilon_i+2\epsilon}=0. \tag{6}$$

Also, the calculated ρ_{calc} value, using the above BEMA approximation, is compared with experimental data ρ_{exp} through the following unbiased estimator:

$$\delta^2=\frac{1}{N}\sum(\rho_{i,exp}-\rho_{i,calc})^2, \tag{7}$$

where N is the number of experimental points. The minimizing procedure gives the best fit of the experimental spectra.

In the present experiments, the SE modeling was performed by including dielectric functions of the c-InP, the InP native oxide, the metallic indium, and voids. In particular, for the dielectric function of c-InP and the voids database provided by Aspnes was used. As for the metallic indium, 1-μm thick film was deposited on quartz substrate by indium evaporation and the corresponding dielectric function was measured.

The single Lorentzian oscillator expression[31] was used to describe the dielectric response of the InP native oxide:

$$\epsilon(\omega)=\epsilon_\infty+\frac{(\epsilon_0-\epsilon_\infty)\omega_0^2}{\omega_0^2-\omega^2+i\Gamma\omega}, \tag{8}$$

where ϵ_∞ is the high-frequency dielectric constant, ϵ_0 is the static dielectric constant (the value of dielectric constant when the frequency ω approaches zero), ω_0 is the resonance frequency, and Γ is the damping constant. By interpolating

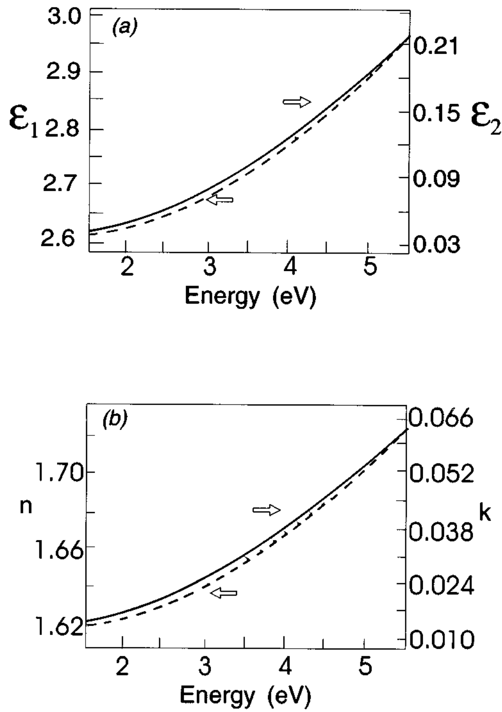

FIG. 1. Energy dependence at $T=25$ °C of (a) the real, ϵ_1, and imaginary, ϵ_2, parts of the dielectric function and of (b) the refractive index n and the extinction coefficient k of the InP native oxide, as obtained by the single Lorentzian oscillator expression (see text).

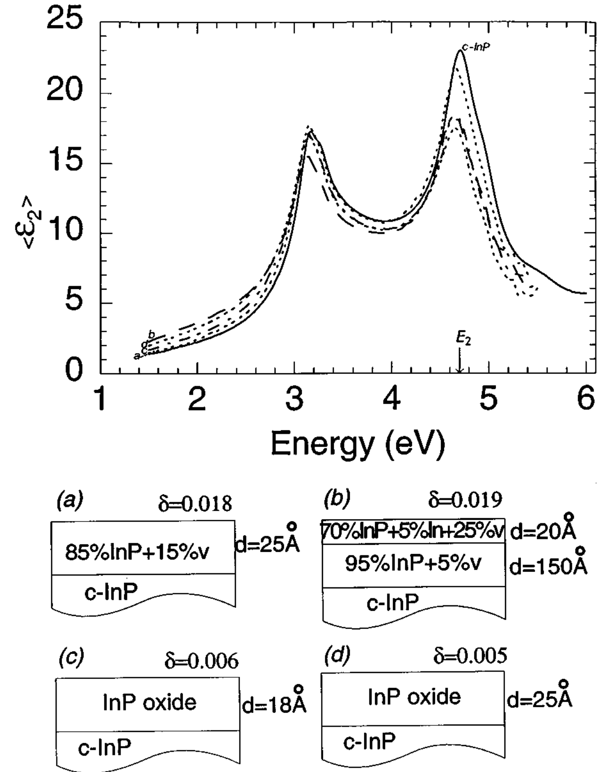

FIG. 2. Top: $\langle\epsilon_2\rangle$ spectra recorded at room temperature for (a) InP substrate exposed to H atoms for 7 min at $T=230$ °C, (b) InP substrate exposed to H atoms at $T=350$ °C for 2 min, (c) InP substrate exposed to H atoms at room temperature for 20 min, and (d) InP substrate covered with 25 Å of native oxide. The E_2 interband critical point at 4.7 eV photon energy is also shown. The reference c-InP spectrum is also shown (solid line). Bottom: best fit BEMA models corresponding to the spectra.

the $\langle\epsilon\rangle$ spectrum of a c-InP substrate covered with a 25-Å native-oxide layer, the following oscillator parameters were derived:

$$\epsilon_\infty = 1,$$

$$\epsilon_0 = 2.5943,$$

$$\omega_0 = 12.1054 \ \ \mathrm{cm}^{-1},$$

$$\Gamma = 2.4194 \ \ \mathrm{cm}^{-1}.$$

The obtained wavelength-dependent dielectric response of the InP native oxide is shown in Fig. 1(a). The real and imaginary parts of the refractive index calculated from the above spectra are reported in Fig. 1(b). Slight differences in the optical properties of the InP native oxide from previous reported data[32] are most likely due to differences in composition and density, since it has been noted that oxides prepared with different techniques tend to have different dielectric responses.

III. RESULTS AND DISCUSSION

A. Oxygen removal: the cleaning process

In order to investigate the oxide reduction kinetics, the hydrogen plasma treatment of InP samples was performed at various times and temperatures, under the same plasma conditions. Figure 2 shows typical $\langle\epsilon_2\rangle$ spectra recorded at room temperature after H atoms treatment at (a) 230 °C for 7 min, (b) 350 °C for 2.5 min, (c) 25 °C for 20 min. In the same figure, the $\langle\epsilon_2\rangle$ spectra of untreated InP substrate [spectrum (d)] and of c-InP database are also shown. The main features of the spectra are the two characteristic InP interband E_1 and E_2 peaks at the photon energies of 3.1 and 4.7 eV,[33,34] respectively. The fact that they are well shaped indicates that, under the above plasma conditions, the possible strong amorphization and metallization (i.e., indium enrichment) can be ruled out. The analysis of these spectra in terms of the best-fit BEMA models is shown in the bottom of Fig. 2. Obviously, among the different models which have been tested for each case, those giving the lowest δ values are also in reasonable accord with composition and morphology data derived by XPS and AFM measurements. In particular, at room temperature and after a hydrogen exposure of 20 min (model c), the simplest model giving the lowest δ value still includes an 18-Å layer of native oxide, whose presence has also been confirmed by XPS analysis. This oxide layer does not further reduce with longer hydrogen exposure time and with increasing the temperature up to 150 °C. On the contrary, at $T=230$ °C, a complete removal of the oxide layer is achieved, by exposing the InP substrate to the H-atoms flux for 7 min. In this case, a single-layer model (model a) including a rough layer of 25 Å, represented by a mixture of 85% c-InP and of 15% voids, gives the lowest δ value. Substantive justification exists for this model based on both the XPS analysis which did not detect oxygen and the AFM image (shown in Fig. 3) which gives an estimated roughness

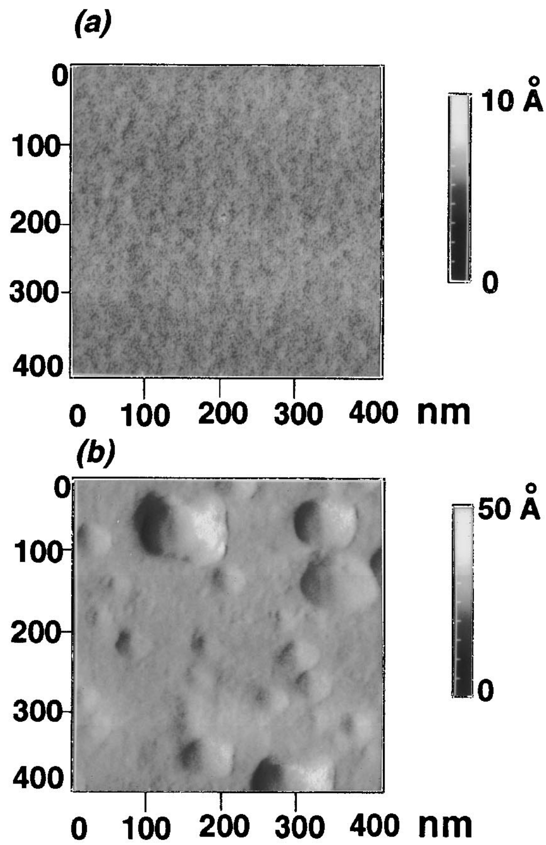

FIG. 3. Top view atomic force microscopy (AFM) images of InP surfaces exposed to hydrogen plasmas (a) at $T=230$ °C for 7 min and (b) at room temperature for 170 min.

of ~30 Å. This roughness value is in reasonable accord with the 25-Å layer measured by SE.

For the treatment at 350 °C, the XPS analysis has evidenced the presence of metallic indium in the In $3d_{5/2}$ peak. Thus, for the best fit of the spectrum (b), both voids and indium enrichment must be included in a single-layer or multilayer model. The lowest δ value has been obtained for a two-layer model including a density deficient inner layer of 150 Å, simulated by a mixture of 95% c-InP and 5% voids, and a porous and indium-rich (70% c-InP, 25% voids, 5% indium) topmost layer 20 Å in thickness. In this case, the kinetics of the damage process is as fast as the oxygen removal, so that the two processes of Eqs. (1) and (2) are almost concomitant, and surface damage is induced even at short plasma exposure time.

The real-time monitoring of the surface modifications has been done by performing ellipsometric measurements at fixed energy of 4.7 eV (E_2 peak). At this energy, the $\langle\epsilon_2\rangle$ value is sensitive to surface modifications as can be seen in Fig. 2. Figure 4 shows the time evolution of $\langle\epsilon_2(E_2)\rangle$ during hydrogen exposure of InP substrates, at temperatures in the range 25–350 °C. For each curve, the initial point corresponds to a c-InP substrate covered with a 25 Å-thick native-oxide layer. Obviously, the higher the temperature the lower the initial $\langle\epsilon_2(E_2)\rangle$ value, since it is well documented[34,35] that a temperature increase induces both a decrease and a shift to low energy of the $\langle\epsilon_2\rangle$ spectrum. The highest $\langle\epsilon_2(E_2)\rangle$ profile obtained for the 230 °C treatment is indicative of an oxide-removal process more effective than that observed at different temperatures. In particular, at 25 °C and 150 °C, a plateau of a lower $\langle\epsilon_2(E_2)\rangle$ value is reached after 15 min and after 5 min, respectively, of exposure to hydrogen plasma, thus indicating an incomplete oxide removal. By contrast, at 350 °C, the $\langle\epsilon_2(E_2)\rangle$ value increases at first, and reaches a maximum after 1.5 min; with longer exposure of the surface, the trend reverses and the E_2 peak starts to decrease since surface damage, mainly phosphorus depletion, occurs.

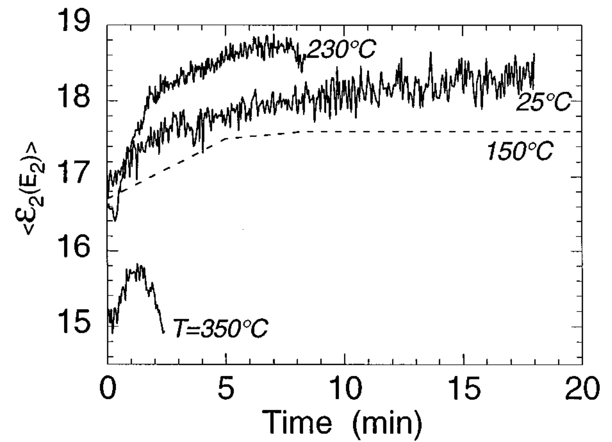

FIG. 4. $\langle\epsilon_2\rangle$ value at the E_2 peak vs rf hydrogen plasma exposure time at different InP surface temperatures. In all the experiments the H-atom flux impinging on the InP substrate was $\sim 4\times10^{20}$ atoms/cm^2 sec.

In order to avoid creation of phosphorus vacancies and, hence, indium enrichment of the InP surface, many authors[6,36] dealing with hydrogen-InP interaction have proposed the use of plasmas fed by PH_3 instead of H_2. Therefore, the effect of PH_3 addition to the hydrogen plasma during the cleaning of InP samples at $T=230$ °C has been investigated. Figure 5 shows the time dependence of the $\langle\epsilon_2\rangle$ value at 4.6 eV (E_2 peak position at $T=230$ °C) during the exposure of the InP surface to PH_3/H_2 plasmas containing different PH_3 amounts. At a PH_3 percentage higher than 0.2%, a $\langle\epsilon_2\rangle$ decrease is observed which becomes faster when

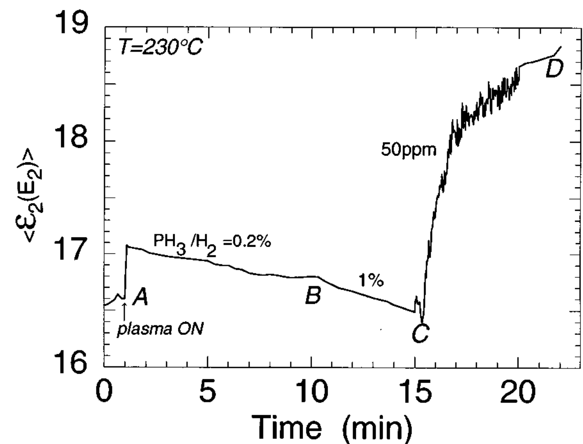

FIG. 5. Time evolution of the $\langle\epsilon_2\rangle$ value at 4.6 eV during the exposure, at $T=230$ °C, of the InP surface to PH_3/H_2 plasmas with different PH_3/H_2 ratio: $PH_3/H_2=0.2\%$ (curve AB), $PH_3/H_2=1\%$ (curve BC), and $PH_3/H_2=50$ ppm (curve CD).

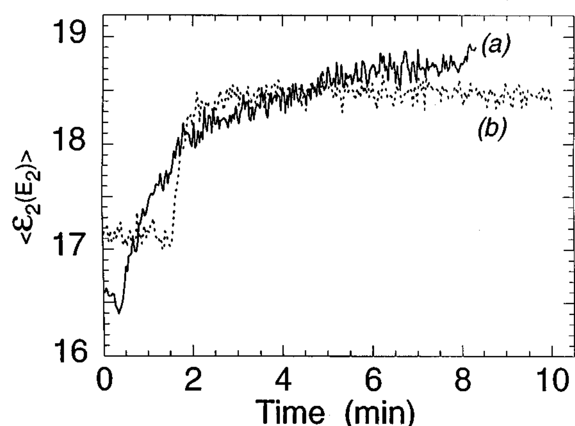

FIG. 6. $\langle\epsilon_2\rangle$ time dependence at the photon energy of 4.6 eV during the hydrogen exposure at the surface temperature of 230 °C of InP substrates (a) without and (b) with wet precleaning by $H_2O:H_2SO_4:H_2O_2=1:8:1$ solution.

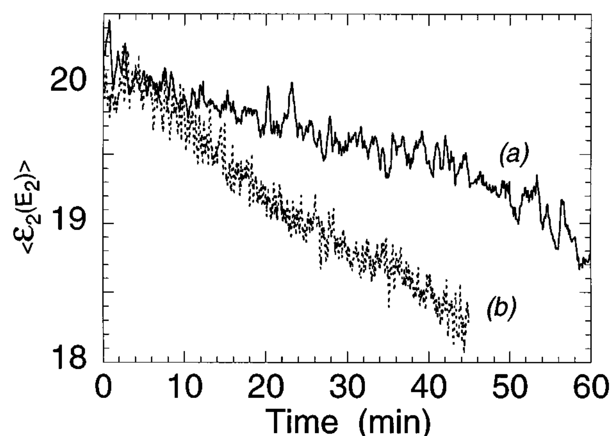

FIG. 7. Time dependence of the $\langle\epsilon_2\rangle$ value at the E_2 peak (4.7 eV) during the hydrogen exposure at room temperature of InP surfaces cleaned by (a) hydrogen plasma for 7 min at $T=230$ °C (solid line) and by (b) oxide thermal desorption at $T=640$ °C (dashed line).

the PH_3/H_2 ratio is increased. This observation indicates that phosphorus deposition occurs on the InP substrate.[3] The presence of the deposited phosphorus subtracts H atoms from the cleaning process (1), because of the concomitant existence of the equilibrium:

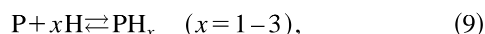

$$P+xH \rightleftarrows PH_x \quad (x=1-3), \tag{9}$$

producing PH_x species on the surface.

The $\langle\epsilon_2\rangle$ value increases when the PH_3 amount in the plasma is about 50 ppm. Under this last condition, the H atoms predominate over the PH_x radicals and, hence, the oxide-reduction process exceeds P deposition. This observation suggests that the PH_3 amount added to H_2 plasmas to stabilize the InP surface has to be appropriately controlled; otherwise it could inhibit the oxygen removal process.

Another trick for optimizing the III-V surface cleaning process is to perform a wet-etching prior to exposing the III-V surface to H atoms.[9,10] Therefore, a wet-etched InP sample has been exposed to hydrogen plasma at the optimum temperature of 230 °C. Figure 6 shows the comparison of the $\langle\epsilon_2(E_2)\rangle$ time evolution for two dry-cleaned InP substrates with and without wet precleaning. It can be seen that the preliminary wet etching causes a faster O-removal kinetics by H atoms, besides a reduction of the native-oxide thickness to 19 Å. The different kinetics could be explained by the different chemical nature of the oxide[2] and by a disordered phase introduced by wet etching.

B. Phosphorus depletion: the damage process

In the above, it has been clearly evidenced that the cleaning process can give a damaged surface when the phosphorus depletion [Eq. (2)] and the oxygen removal [Eq. (1)] are concomitant processes. Figure 7 shows the effect of the exposure time on the $\langle\epsilon_2\rangle$ maximum during the hydrogenation, at room temperature, of two oxide-free InP samples. These differently cleaned InP samples have been obtained as follows: (a) the oxide has been removed by H-atom exposure for few minutes at $T=300$ °C followed by thermal annealing at $T=430$ °C; (b) the oxide has been removed by thermal desorption at $T=640$ °C. For both samples, the observed decrease of the $\langle\epsilon_2(E_2)\rangle$ value is consistent with the formation of a rough and indium-rich overlayer of increasing porosity and/or thickness, which is faster in sample (b). Thus, the extent of damage depends on the sample history. This result can be related to the presence of a more disordered phosphorus-phase, induced by the high annealing temperature, containing weak In-P bonds or P-interstitial atoms which are more reactive toward H atoms.

The evaluation of the InP surface modifications caused by the prolonged exposure to H atoms has been done through the $\langle\epsilon_2\rangle$ spectra recorded at the selected treatment time of 45, 80, and 170 min during the experiment (a) of Fig. 7. These spectra are shown in Fig. 8 plus the results of the corresponding BEMA modeling. The three-layer model, in which indium percentage, roughness, and thickness of the layers increase with exposure time, provides the best fit of the $\langle\epsilon_2\rangle$ spectra. The choice of this model is also supported by XPS and AFM measurements. In fact, the angle-resolved XPS analysis on the In $3d_{5/2}$ peak has shown an in-depth profile of metallic indium percentage, whose value was very high in the first 7–20 Å. Also, the AFM image [see Fig. 3(b)] of a typical high-damage sample shows a very rough surface with craters and droplets.

As for the substrate temperature, a strong effect has also been observed on the kinetics of the surface damage. Figure 9 shows the E_2 peak evolution, as recorded during H-atom exposure at various temperatures between 25 and 350 °C. The obtained data show that H-atom treatment performed in the range $(25<T<70)$ °C slightly lowers the InP dielectric function. For $(70<T<100)$ °C the dielectric function of InP is not altered and, in particular, the damage of InP surface is minimized at $T=100$ °C. This result agrees well with that reported by de Pierry *et al.*,[14] who obtained a damage-free InP surface performing the H-atom treatment at $T=90$ °C. Above 100 °C, the higher the temperature the faster the damage. These data suggest that at temperatures below 100 °C hydrogen atoms create microroughness and isolated P vacancies, whereas at temperatures higher than 100 °C, the surface rapidly deteriorates with the formation of indium droplets.

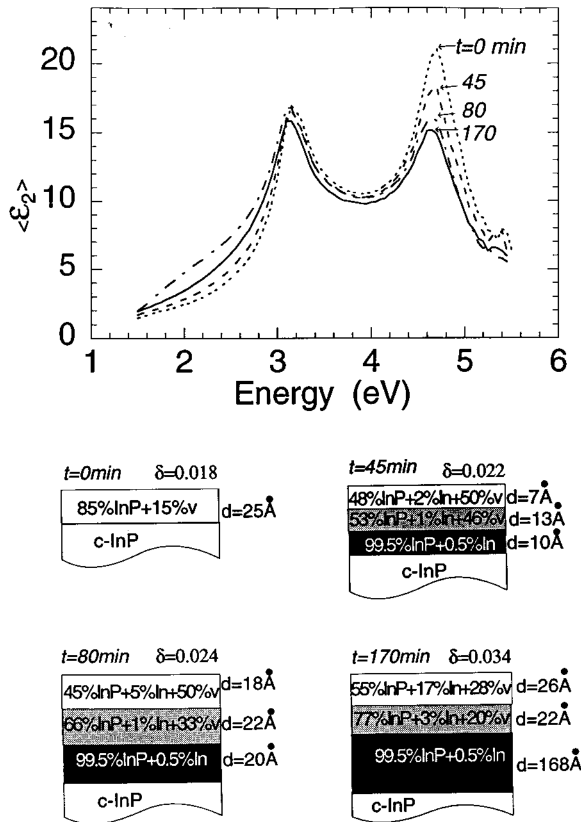

FIG. 8. Top: imaginary part, $\langle \epsilon_2 \rangle$, of the pseudodielectric function of cleaned InP samples before (----) and after exposure to hydrogen plasma at room temperature for 45 min (– –), 80 min (-···) and 170 min (—). Bottom: damage depth and composition of hydrogen exposed samples calculated from the corresponding $\langle \epsilon_2 \rangle$ spectra at room temperature by BEMA modeling.

However, when the damage induced by H atoms is confined to the InP surface and does not involve the bulk material, it can be recovered by thermal annealing at $T=430$ °C under PH_3 overpressure. In fact, the damaged samples were annealed, for 10 min, in the presence of PH_3, at the temperatures of 150, 300, and 430 °C. The samples heated at 150–300 °C do not show any significant improvement of the $\langle \epsilon_2 \rangle$ spectra, whereas the sample heated at 430 °C shows a sharp increase of the E_2 peak (see Fig. 10) and, the corresponding $\langle \epsilon_2 \rangle$ spectrum exactly coincides with that of a damage-free InP surface (see inset of Fig. 10). Thus, at 430 °C, PH_3 thermally decomposes on the surface, producing P species, mainly P_4 and P_2H_4,[25] available to saturate the P vacancies and reconstruct the InP surface.

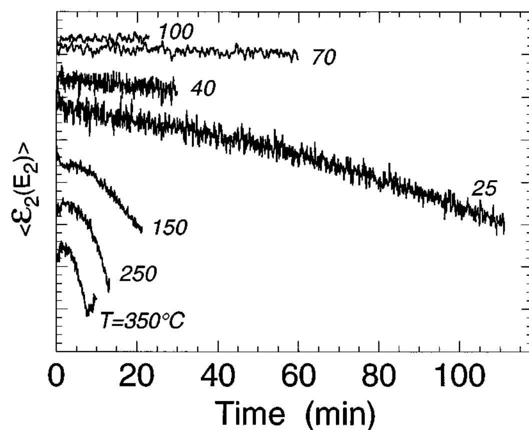

FIG. 9. Trends of the $\langle \epsilon_2 \rangle$ value at the E_2 maximum vs time during hydrogen plasma exposure of a clean InP surface at various substrate temperatures.

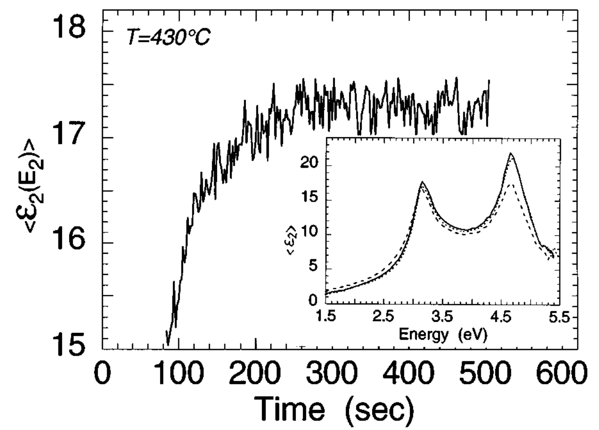

FIG. 10. $\langle \epsilon_2 \rangle$ absolute maximum trend at 4.6 eV vs annealing time for hydrogenated InP samples during annealing at $T=430$ °C in presence of few ppm of phosphine. The inset shows the SE spectrum recorded before (– –) and after annealing (-----), compared to that of a clean InP sample (—).

C. Chemistry and kinetics

The ellipsometric data have clearly evidenced that the occurrence of both O-removal [Eq. (1)] and P-depletion [Eq. (2)] processes strongly depends on the treatment time, on the surface nature, and on the temperature apart from the H-atom density. Among these parameters, the surface temperature is the key of the process chemistry. In particular, the temperature dependence of the surface reaction rate (Arrhenius-like plot) represents, together with the kinetic profiles, the way to identify the steps controlling the overall surface kinetics. Thus, it is necessary to define, at first, the better way for expressing the rate of the surface reactions. The oxide removal rate, $r_{ox}=\Delta d_{ox}/\Delta t$, has been evaluated from the time dependence of the oxide thickness, d_{ox}, as shown in Fig. 11. Here, the time dependence of the oxide thickness has been derived from the corresponding $\langle \epsilon_2 \rangle$ dependence upon time through the already described BEMA models. Analogously, the P-depletion rate, $r_P=\Delta V_{In+void}/\Delta t$, has been deduced by the time variation of the total indium+void volume fraction reported in Fig. 12.

The observed linear time dependence of the oxide thickness and of the damage shown in Figs. 11 and 12 suggests that both processes of O removal and P ablation are not controlled by the diffusion of hydrogen into InP (otherwise a $t^{1/2}$ dependence should be observed) whatever the surface temperature.[37] Moreover, the same linear behavior of Fig. 11 indicates that the oxide-reduction process is not limited even by H_2O out-diffusion at $T>230$ °C. It seems that, at high temperatures, the rate-limiting step of the O-removal process is rather the surface interaction of H atoms with —In—O—

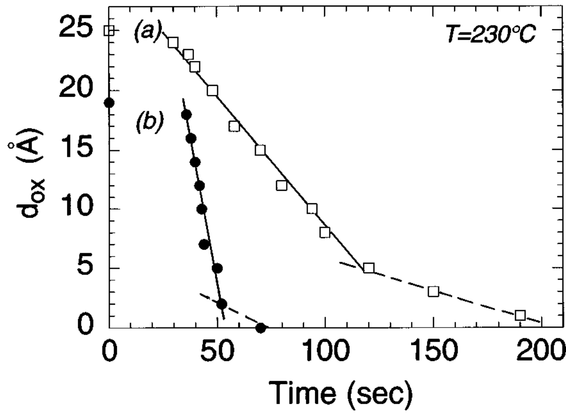

FIG. 11. Thickness of the native oxide layer vs time during H atoms exposure at $T=230$ °C, calculated by BEMA modeling, for (a) the dry cleaned sample (measured O-reduction rate $r_{ox}=0.22$ Å/sec), and (b) the preliminar wet etched sample by H_2O:H_2SO_4:H_2O_2=1:8:1 solution (measured O-reduction rate $r_{ox}=0.98$ Å/sec). See also Fig. 6.

and —P—O— bonds which react faster than the —In—O— bonds, as similarly reported in literature for GaAs oxide.[17] This hypothesis is consistent with the strong effect of the oxide composition on the O-removal rate as shown in Fig. 11. In fact, the two different slopes for sample (a) and (b) and, hence, the different O-removal rate of 0.22 and 0.98 Å/sec are the consequence of a higher amount of phosphorus oxides in sample (b) than in sample (a). In this last, the indium is more oxidized than phosphorus, as revealed by previous XPS analysis.[2] Moreover, the sharp rate change observed for both the samples in Fig. 11 when the oxide thickness has been reduced to 3–4 Å, is due to the slower reduction kinetics of the In_2O_3 inner layer[2] with respect to the faster reduction kinetics of the P-O-rich outmost layer. At low temperatures, the surface chemistry and kinetics can also be controlled by the adsorption of water according to similar reactions reported for GaAs by Gottscho:[15]

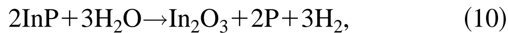

$$2InP+3H_2O \rightarrow In_2O_3+2P+3H_2, \tag{10}$$

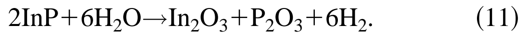

$$2InP+6H_2O \rightarrow In_2O_3+P_2O_3+6H_2. \tag{11}$$

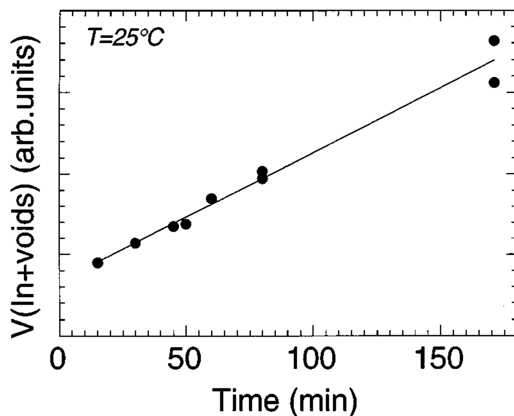

FIG. 12. InP damage, expressed in terms of the total indium +voids volume fraction, $V_{(In+voids)}$, as induced by H atoms vs hydrogen exposure time at room temperature for a clean InP sample.

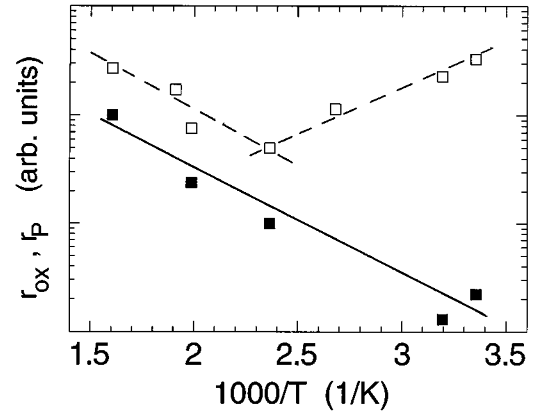

FIG. 13. Arrhenius-like plot of the O-removal rate, $\Delta d_{ox}/\Delta t$ (■) and P-depletion rate $\Delta V_{In+voids}/\Delta t$ (□) as defined in the text.

Hence, at $T<130$ °C the In_2O_3 layer and the H_2O occupying sites which are not available for H atoms, act as a barrier for the further interaction of H atoms with both O and P sites so impeding the total oxide reduction. Therefore, a constant $\langle\epsilon_2\rangle$ value is maintained even at long hydrogen treatment time when at $T=25$ °C and $T=150$ °C (see Fig. 4). On the contrary, at $T>230$ °C, H_2O easily desorbes and a complete oxide reduction can be achieved so leaving a perfectly cleaned InP surface which is no longer protected by oxygen atoms and/or H_2O. After that, the InP surface could undergo the degradation process (2) if the H-atom exposure is not immediately stopped, as evidenced by the sudden decrease of the $\langle\epsilon_2\rangle$ value in Fig. 4.

Hence, a key issue for a successful cleaning is the end-point detection i.e., the possibility to stop the exposure to H atoms before InP degradation can occur. Fortunately, our results show that InP damage only starts when the oxygen has been completely removed. Therefore, the time dependence of the $\langle\epsilon_2\rangle$ value can be easily used to define the boundary layer between processes (1) and (2). Similarly, Hu *et al.*[21] have shown that the (Ψ,Δ) trajectory can also be used for the end-point detection of the native-oxide removal from Si surface to obtain bare Si without damage.

The chemical model of the oxygen-removal and phosphorus-depletion processes should include: (i) the supply of the H atoms to the InP surface and (ii) the interaction of the H atoms with the InP surface. Under the present experimental conditions, i.e., high H-atom flux and the small area of the exposed InP surface, the supply of H atoms can be excluded as a rate-controlling step. The interaction of H atoms with the InP surface takes place in the kinetic region, i.e., the rates of both the O-removal and P-ablation processes depend on the H-atom coverage ($r=k\theta_H$), and the temperature affects the pseudorate constant k^* of the surface reactive process according to the Arrhenius law:

$$k^*=A\ \exp\left(-\frac{E_a^*}{RT}\right), \tag{12}$$

where E_a^* is the pseudoactivation energy of the surface reactive process. The temperature dependence of the O-removal rate, dd_{ox}/dt, and of the P-depletion rate, $d(\mathrm{In}+\mathrm{voids})/dt$, is shown in the Arrhenius-like plot of Fig. 13. The O-removal process is characterized by a single pseudo-

activation energy, E_a^*, of 0.20 ± 0.05 meV. In contrast, the P-depletion process is characterized by a positive pseudoactivation energy of $+0.20 \pm 0.05$ eV at high temperatures, and by a negative pseudoactivation energy of -0.15 ± 0.05 eV at low temperatures. However, the derived pseudoactivation energies are too low to be attributed to a reactive step only, and, hence, they are not the ''true'' activation energies. In fact, the interaction of H atoms with InP has basically three steps: the chemisorption of H atoms on active sites, the chemical reaction, and the desorption of the reaction products. Therefore, the chemical schemes corresponding to the O-removal and P-depletion processes should be written as

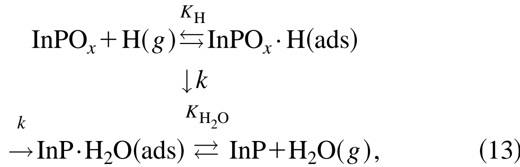

$$InPO_x + H(g) \overset{K_H}{\leftrightarrows} InPO_x \cdot H(ads) \downarrow k \overset{k}{\rightarrow} InP \cdot H_2O(ads) \overset{K_{H_2O}}{\rightleftarrows} InP + H_2O(g), \quad (13)$$

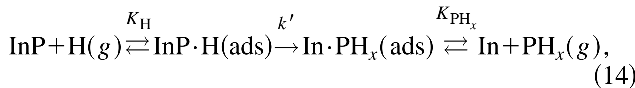

$$InP + H(g) \overset{K_H}{\rightleftarrows} InP \cdot H(ads) \overset{k'}{\rightarrow} In \cdot PH_x(ads) \overset{K_{PH_x}}{\rightleftarrows} In + PH_x(g), \quad (14)$$

where K_H is the constant for the chemisorption equilibrium of H atoms, K_{H_2O} and K_{PH_x} are the constants for the desorption equilibrium of the reaction products H_2O and PH_x, and k is for the rate constant of the reactive step. From the kinetic point of view the above chemical models are a specific case in which the reaction product (H_2O, PH_x) inhibits the reaction, since some active sites are occupied by the products. When this hypothesis applies, the true activation energies, E_a, are reduced by the heat of adsorption of hydrogen atoms, Q_H, and increased by the product adsorption heats, which are Q_{H_2O} and Q_{PH_x} ($x = 1-3$) in the O-removal and P-ablation processes, respectively. Thus, it can be written:

$$E_a^* = E_a - Q_H + Q_{H_2O}, \quad (15)$$

$$E_a^* = E_a' - Q_H + Q_{PH_x}, \quad (16)$$

for the pseudoactivation energy E_a^* and $E_a'^*$ of O-removal and P-depletion processes, respectively.

The fact that the P depletion presents two different thermal activation zones can be explained on the basis of two different species desorbing from the InP surface, PH_3 at low temperatures and PH at high temperatures, according to the reactions:

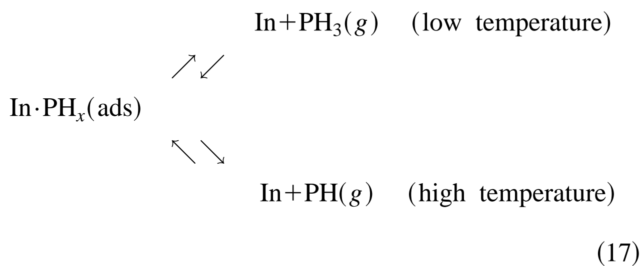

$$In \cdot PH_x(ads) \rightleftarrows In + PH_3(g) \quad \text{(low temperature)}; \quad In \cdot PH_x(ads) \rightleftarrows In + PH(g) \quad \text{(high temperature)} \quad (17)$$

At high temperatures (positive pseudoactivation energy) the surface is sparsely covered by H atoms and, hence, PH is formed and desorbed; whereas at low temperatures (negative pseudoactivation energy) the surface is well covered by H atoms and PH_3 is formed which easily desorbs. This explanation is also supported by the opposite value of the adsorption heats[38] being negative ($Q_{PH_3} = -24 \pm 5$ kcal/mol) for PH_3 and positive ($Q_{PH} = +26 \pm 5$ kcal/mol) for PH: the endothermic PH_3 adsorption and the exothermic PH adsorption contribute to the decrease and to the increase of the pseudoactivation energy [see Eq. (16)], respectively. This anomalous behavior of the E_a^* has already been evidenced in the etching of GaAs by Cl_2 plasma.[39,40]

IV. SUMMARY AND CONCLUSIONS

Radio-frequency hydrogen plasmas were used to investigate the interaction of H atoms with the InP surface and aimed to study (a) the oxygen removal of the surface native oxide, for the substrate cleaning (*the cleaning process*) and (b) the phosphorus depletion from the InP bulk which causes material damage (*the damage process*).

Using an *in situ* phase-modulated spectroscopic ellipsometer, the InP surface under treatment was continuously monitored in real time and its modification recorded in terms of $\langle \epsilon_2 \rangle$. The ellipsometric spectra gave the fingerprint of the outmost surface layers in terms of oxide layer thickness and void composition, and of thickness of the phosphorus depleted layer. In addition, the time evolution of the ellipsometric data allowed the kinetics of the surface process to be quantified.

The cleaning process was found to strongly depend on surface temperature. In particular, (a) at low temperature ($T < 150$ °C) the oxygen-removal process stopped after the first few angstroms (5–10 Å) of cleaning as the H_2O desorption from the inner layer did not occur completely; (b) at intermediate temperature ($T \approx 200$ °C) a complete removal of the oxide layer was obtained. Typically, at 230 °C the removal of 25 Å of native oxide was obtained after 7 min of H_2 plasma treatment and the resulting outmost surface layer included 20% of voids only. Once the oxygen was completely removed, the H atoms became available for the phosphorus depletion and the InP surface could be damaged from further exposure; (c) at high temperature ($T > 250$ °C) the oxygen removal became more rapid and it was not discernible from the phosphorus-depletion process which was also rapid. The outmost surface layers included, beside voids, phosphorus vacancies.

The overall rate of the surface process, for both oxygen removal (r_{ox}) and phosphorus depletion (r_P) displayed Arrhenius behavior at various temperatures as follows: for the cleaning process, $r_{ox}(T)$ had a monotonous curve, i.e., the rate increased with increasing temperature (RT–350 °C) and the resulting activation energy was 0.20 ± 0.05 eV; for the damage process, the phosphorus depletion rate $r_P(T)$ had a nonmonotonous curve, i.e., the $r_P(T)$ curve presented a minimum, and two values of activation energy were measured; the first value was negative (-0.15 ± 0.05 eV) in the low-temperature zone (RT–200 °C) and, the second was positive (0.20 ± 0.05 eV) in the high-temperature zone (200–350 °C).

The low value of the activation energy and the fact that different activation energy values, depending on the temperature range, could be measured for the same surface reactive process was not surprising, considering that in the heterogeneous processes the temperature dependence of the

reactive surface process is the result of the concurrence of several elementary processes. In particular, the suggested chemical model included for the oxygen-removal process the desorption of H_2O and, for the phosphorus depletion, the desorption of PH_3 in the low-temperature zone and of PH in the high-temperature zone, apart from H-atom chemisorption and reactive steps.

ACKNOWLEDGMENTS

We express our gratitude to Professor Eugene A. Irene of University of North Carolina for the helpful discussion regarding ellipsometric modeling. The authors wish to thank Dr. A. Ciancio of Istituto di Nematologia Agraria-C.N.R for AFM measurements.

[1] A. Guivarc'h, H. L'Haridon, G. Pelous, G. Hollinger, and P. Pertosa, J. Appl. Phys. **55**, 1139 (1984).
[2] M. Losurdo, G. Bruno, and P. Capezzuto, J. Vac. Sci. Technol. B **14**, 691 (1996).
[3] H. Ninomiya, T. Sugino, K. Matsuda, and J. Shirafuji, Jpn. J. Appl. Phys. **32**, L12 (1993).
[4] E. M. Omeljanovsky, A. V. Pakhomov, and A. Y. Polyakov, Semicond. Sci. Technol. **4**, 947 (1989).
[5] S. Balasubramanian, K. S. R. Koteswara Rao, N. B. Balasubramanian, and V. Kumar, J. Appl. Phys. **77**, 5398 (1995).
[6] T. Sugino, H. Yamamoto, and J. Shirafuji, Jpn. J. Appl. Phys. **30**, L948 (1991).
[7] W. C. Dautremont-Smith, J. Lopada, S. J. Pearton, L. A. Koszi, and M. Stavola, J. Appl. Phys. **66**, 1993 (1989).
[8] E. J. Petit, F. Houzay, and J. M. Moison, Surf. Sci. **269/270**, 902 (1992).
[9] E. J. Petit and F. Houzay, J. Vac. Sci. Technol. B **12**, 547 (1994).
[10] E. J. Petit, F. Houzay, and J. M. Moison, J. Vac. Sci. Technol. A **10**, 2172 (1992).
[11] C. W. Tu, R. P. H. Chang, and A. R. Schlier, Appl. Phys. Lett. **41**, 80 (1982).
[12] I. Aller and H. L. Hartnagel, J. Electrochem. Soc. **140**, 2172 (1993).
[13] P. G. Hofstra, D. A. Thompson, B. J. Robinson, and R. W. Streater, J. Vac. Sci. Technol. B **11**, 985 (1993).
[14] P. de Mierry, P. Etchegoin, and M. Stutzmann, Phys. Rev. B **49**, 5283 (1994).
[15] E. S. Aydil, Z. H. Zhou, R. A. Gottscho, and Y. J. Chabal, J. Vac. Sci. Technol. B **13**, 258 (1995).
[16] E. S. Aydil, K. P. Giapis, R. A. Gottscho, V. M. Donnelly, and E. Yoon, J. Vac. Sci. Technol. B **11**, 195 (1993).
[17] R. A. Gottscho, B. L. Preppernau, S. J. Pearton, A. B. Emerson, and K. P. Giapis, J. Appl. Phys. **68**, 440 (1990).
[18] B. Drevillon, E. Bertran, P. Alnot, J. Olivier, and M. Razeghi, J. Appl. Phys. **60**, 3512 (1986).
[19] A. Canillas, E. Bertran, J. L. Andjar, and B. Drevillon, J. Appl. Phys. **68**, 2752 (1990).
[20] E. A. Irene, Thin Solid Films **233**, 96 (1993).
[21] Y. Z. Hu, P. P. Buaud, L. Spanos, Y. Q. Wang, M. Li, and E. A. Irene, J. Vac. Sci. Technol. A **12**, 1315 (1994).
[22] Y. Z. Hu, M. Li, Y. Q. Wang, E. A. Irene, M. C. Hugon, F. Varnier, N. Jiang, M. Froment, and B. Agius, J. Vac. Sci. Technol. B **13**, 227 (1995).
[23] Y. Z. Hu, J. Joseph, and E. A. Irene, J. Vac. Sci. Technol. B **12**, 540 (1994).
[24] Y. Z. Hu, M. Li, E. A. Irene, M. Rowe, and H. C. Casey, Appl. Phys. Lett. **63**, 1113 (1993).
[25] G. Bruno, M. Losurdo, and P. Capezzuto, J. Vac. Sci. Technol. A **13**, 349 (1995).
[26] G. Bruno, M. Losurdo, and P. Capezzuto, Appl. Phys. Lett. **66**, 3573 (1995).
[27] S. N. Jasperson and S. E. Schnatterly, Rev. Sci. Instrum. **40**, 761 (1969).
[28] B. Drevillon, J. Perrin, R. Harbot, A. Violet, and J. L. Dolby, Rev. Sci. Instrum. **53**, 969 (1982).
[29] O. Acher, E. Bigan, and B. Drevillon, Rev. Sci. Instrum. **60**, 65 (1989).
[30] D. A. G. Bruggeman, Ann. Phys. (Leipzig) **24**, 636 (1935).
[31] A. Roseler, *Infrared Spectroscopic Ellipsometry* (Akademie-Verlag, Berlin, 1990).
[32] S. Zollmer, Appl. Phys. Lett. **63**, 2523 (1993).
[33] D. E. Aspnes and A. A. Studna, Phys. Rev. B **27**, 985 (1993).
[34] P. Lautenschlager, M. Garriga, and M. Cardona, Phys. Rev. B **36**, 4813 (1987).
[35] Y. Z. Hu, J. Joseph, and E. A. Irene, J. Vac. Sci. Technol. A **11**, 1786 (1993).
[36] T. Sugino, Y. Sakamoto, T. Sumiguchi, K. Nomoto, and J. Shirafuji, Jpn. J. Appl. Phys. **32**, L1196 (1993).
[37] S. J. Pearton, J. W. Corbett, and J. T. Borenstein, Physica B **170**, 85 (1991).
[38] S. Vepřek, Pure Appl. Chem. **48**, 163 (1976).
[39] H. Deutsch, H. Kersten, and A. Rutscher, Contrib. Plasma Phys. **29**, 263 (1989).
[40] M. Baloch, D. R. Olander, and W. J. Siekhaus, J. Vac. Sci. Technol. B **4**, 794 (1986).